REFERENCES AND NOTES

1. X. Ni, Y. Hu, Y. Wang, C. Li, *Anthropol. Sci.* **113**, 3–9 (2005).
2. K. C. Beard, *Proc. Natl. Acad. Sci. U.S.A.* **105**, 3815–3818 (2008).
3. M. Köhler, S. Moyà-Solà, *Proc. Natl. Acad. Sci. U.S.A.* **96**, 14664–14667 (1999).
4. E. R. Seiffert, *Folia Primatol. (Basel)* **78**, 314–327 (2007).
5. I. S. Zalmout *et al.*, *Nature* **466**, 360–364 (2010).
6. E. R. Seiffert, *Evol. Anthropol.* **21**, 239–253 (2012).
7. N. J. Stevens *et al.*, *Nature* **497**, 611–614 (2013).
8. J. Meng, M. C. McKenna, *Nature* **394**, 364–367 (1998).
9. J. Sun *et al.*, *Sci. Rep.* **4**, 7463 (2014).
10. X. Ni, K. C. Beard, J. Meng, Y. Wang, D. L. Gebo, *Am. Mus. Novit.* **3571**, 1–11 (2007).
11. B. Wang, *Vertebrata PalAsiatica* **46**, 81–89 (2008).
12. X. Ni *et al.*, *Proc. R. Soc. B Biol. Sci.* **277**, 247–256 (2010).
13. K. C. Beard, T. Qi, M. R. Dawson, B. Wang, C. Li, *Nature* **368**, 604–609 (1994).
14. K. C. Beard *et al.*, *Proc. R. Soc. B Biol. Sci.* **276**, 3285–3294 (2009).
15. L. Marivaux *et al.*, *Science* **294**, 587–591 (2001).
16. L. Marivaux, J. L. Welcomme, S. Ducrocq, J. J. Jaeger, *J. Hum. Evol.* **42**, 379–388 (2002).
17. L. Marivaux *et al.*, *Proc. Natl. Acad. Sci. U.S.A.* **102**, 8436–8441 (2005).
18. O. Maridet, X. Ni, *J. Vertebr. Paleontol.* **33**, 185–194 (2013).
19. J. Jaeger *et al.*, *Science* **286**, 528–530 (1999).
20. K. C. Beard, J. Wang, *J. Hum. Evol.* **46**, 401–432 (2004).
21. P. D. Gingerich, A. Sahni, *Nature* **279**, 415–416 (1979).
22. X. Ni, in *Palaeovertebrata Sinica. Volume III. Basal Synapsids and Mammals. Fascicle 3 (Serial no. 16). Eulipotyphlans, Proteutheres, Chiropterans, Euarchontans, and Anagalids*, C. Li, Z. Qiu, Eds. (Science Press, 2015), pp. 284–389.
23. J. X. Samuels, L. B. Albright, T. J. Fremd, *Am. J. Phys. Anthropol.* **158**, 43–54 (2015).
24. A. Licht *et al.*, *Nature* **513**, 501–506 (2014).
25. R. J. Morley, in *Tropical Rainforest Responses to Climatic Change*, M. Bush, J. Flenley, W. Gosling, Eds. (Springer-Verlag, ed. 2, 2011), chap. 1, pp. 1–34.
26. E. R. Seiffert *et al.*, *Proc. Natl. Acad. Sci. U.S.A.* **107**, 9712–9717 (2010).
27. Y. Chaimanee *et al.*, *Proc. Natl. Acad. Sci. U.S.A.* **109**, 10293–10297 (2012).

ACKNOWLEDGMENTS

This project has been supported by the Strategic Priority Research Program of CAS (CAS, XDB03020501), the National Basic Research Program of China (2012CB821904), the CAS 100-talent Program, the National Natural Science Foundation of China (41472025), and the U.S. National Science Foundation (BCS 0820602, BCS 1441585, and EAR 1543684). We thank Z. Yan, G. Wang, R. Li, and G. Li for their assistance in the field. The phylogenetic data used in the paper are archived in the supplementary materials.

SUPPLEMENTARY MATERIALS

www.sciencemag.org/content/352/6286/673/suppl/DC1
Materials and Methods
Systematic Paleontology
Measurements
Body Mass Estimation
Phylogenetic Analysis
Figs. S1 to S10
Tables S1 and S2
References (*28*–*63*)
Databases S1 and S2

7 January 2016; accepted 24 March 2016
10.1126/science.aaf2107

ASTROPARTICLE PHYSICS

Observation of the ^{60}Fe nucleosynthesis-clock isotope in galactic cosmic rays

W. R. Binns,[1]* M. H. Israel,[1]* E. R. Christian,[2] A. C. Cummings,[3] G. A. de Nolfo,[2] K. A. Lave,[1] R. A. Leske,[3] R. A. Mewaldt,[3] E. C. Stone,[3] T. T. von Rosenvinge,[2] M. E. Wiedenbeck[4]

Iron-60 (^{60}Fe) is a radioactive isotope in cosmic rays that serves as a clock to infer an upper limit on the time between nucleosynthesis and acceleration. We have used the ACE-CRIS instrument to collect 3.55×10^5 iron nuclei, with energies ~195 to ~500 mega–electron volts per nucleon, of which we identify 15 ^{60}Fe nuclei. The ^{60}Fe/^{56}Fe source ratio is $(7.5 \pm 2.9) \times 10^{-5}$. The detection of supernova-produced ^{60}Fe in cosmic rays implies that the time required for acceleration and transport to Earth does not greatly exceed the ^{60}Fe half-life of 2.6 million years and that the ^{60}Fe source distance does not greatly exceed the distance cosmic rays can diffuse over this time, ≲1 kiloparsec. A natural place for ^{60}Fe origin is in nearby clusters of massive stars.

Signature of recent nucleosynthesis

The radioactive isotope ^{60}Fe [which decays by β^- decay with a half-life of 2.62×10^6 years (*1*)] is expected to be synthesized and ejected into space by supernovae, and thus could be present in galactic cosmic rays (GCRs) near Earth, depending upon the time elapsed since nucleosynthesis and the distance of the supernovae. ^{60}Fe is believed to be produced primarily in core-collapse supernovae of massive stars with mass $M >$ ~10 solar masses ($M_\odot$), which occur mostly in associations of massive stars (OB associations). It is the only primary radioactive isotope with atomic number $Z \leq 30$ [with the exception of ^{59}Ni, for which only an upper limit is available (*2*)] produced with a half-life long enough to potentially survive the time interval between nucleosynthesis and detection at Earth. (Primary cosmic rays are those that are synthesized at the GCR source, as opposed to secondary cosmic rays, which are produced by nuclear interactions in the interstellar medium.) ^{60}Fe is difficult to measure with present-day instruments because of its expected extreme rarity, based on nucleosynthesis calculations for supernovae (*3*, *4*). The detection of ^{60}Fe in cosmic rays would be a clear sign of recent, nearby nucleosynthesis. The long period of data collection (17 years) achieved by the Cosmic Ray Isotope Spectrometer (CRIS) aboard NASA's Advanced Composition Explorer (ACE) (*5*), the excellent mass and charge resolution of the CRIS instrument, and its capability for background rejection have enabled us to detect ^{60}Fe.

^{60}Fe has been detected in other samples of matter. Measurements of diffuse γ-rays from the interstellar medium (ISM) by the spectrometer on the International Gamma-Ray Astrophysics Laboratory (INTEGRAL) spacecraft have revealed line emission at 1173 and 1333 keV from ^{60}Co, the daughter product of ^{60}Fe decay, clear evidence that "nucleosynthesis is ongoing in the galaxy" (*6*). As expected, this emission is diffuse instead of point-like, since the ^{60}Fe lifetime is sufficiently long to allow it to diffuse over distances that are large compared to the size of a supernova remnant. This is one of many strong connections between γ-ray astronomy and direct cosmic-ray studies (*7*).

Deep-sea manganese crusts from two different locations have also been found to harbor elevated ^{60}Fe levels (*8*, *9*). Analysis of crust layers using accelerator mass spectrometry showed significant increases in the ^{60}Fe/Fe ratio 2.8 million years (My) ago, "compatible with deposition of supernova ejecta at a distance of a few tens of pc" (*9*). The measurement was verified by an independent analysis (*10*), although these investigators did not find a corresponding increase in a marine-sediment sample [see (*10*, *11*) for discussion]. We note that the manganese crust studies (*8*–*10*) used outdated half-lives for ^{60}Fe and ^{10}Be—1.49 and 1.51 My , respectively—instead of the currently accepted 2.62 and 1.387 My (*1*). Using these recent lifetimes, it has been estimated that the peak in the ^{60}Fe/Fe ratio (*9*) as a function of depth corresponds to an age of 2.2 My (*11*). Lunar surface samples also show elevated ^{60}Fe/Fe ratios consistent with supernova debris arriving on the Moon ~2 My ago (*12*, *13*). These deep-sea manganese crust and lunar surface observations were compared with expectations from possible stellar sources (*11*) and found to be consistent with an origin in core-collapse supernovae, but inconsistent with Type Ia supernovae, which produce orders of magnitude less ^{60}Fe.

Cosmic-ray ^{60}Fe detection

The CRIS instrument was launched on ACE in 1997 and has operated continuously since that

[1]Washington University, St. Louis, MO 63130, USA. [2]NASA/Goddard Space Flight Center, Greenbelt, MD 20771, USA. [3]California Institute of Technology, Pasadena, CA 91125, USA. [4]Jet Propulsion Laboratory, California Institute of Technology, Pasadena, CA 91109, USA.
*Corresponding author: Email: wrb@wustl.edu (W.R.B.); mhi@wustl.edu (M.H.I.)

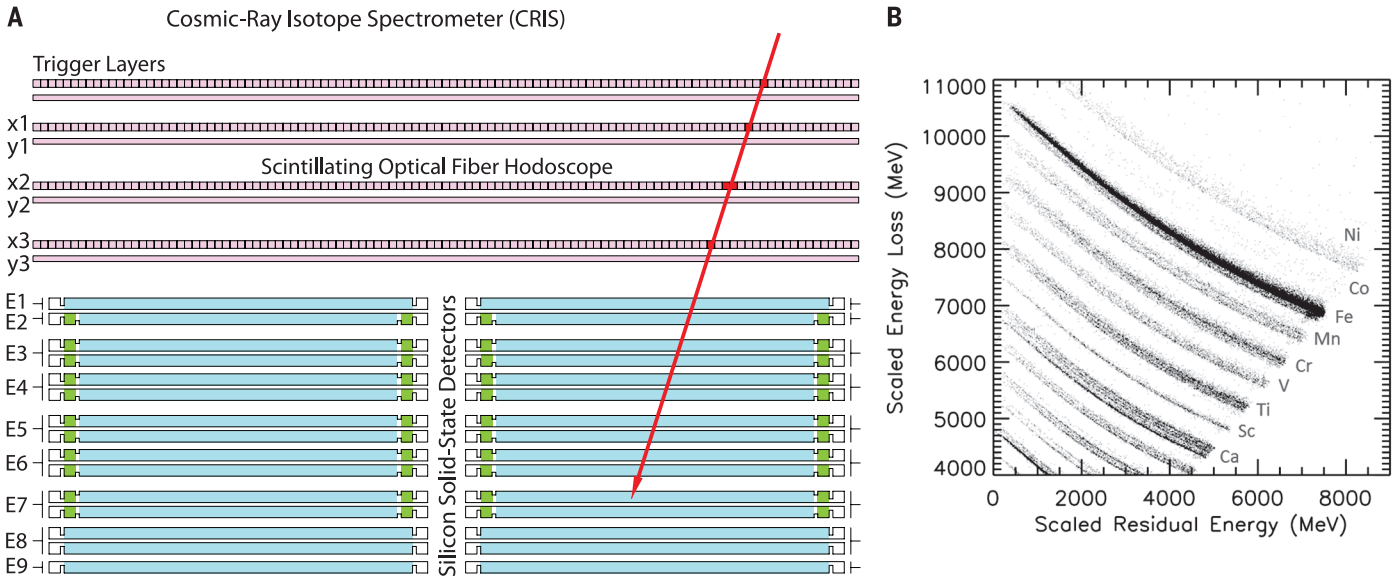

Fig. 1. CRIS instrument and data sample. (**A**) A cross-section drawing (not to scale) of the CRIS instrument is shown. There are four x,y planes of fibers; the top plane provides a trigger signal and the next three planes (x1y1,x2y2, x3y3) provide the trajectory. Beneath the fibers are four stacks of 15, 3-mm-thick silicon detectors (two stacks are visible in this side view). The central active regions of the silicon detectors are shown in blue, and guard rings used to veto side-exiting particles are in green. The detectors are grouped so that up to nine energy-loss signals (E1 to E9) are obtained for each particle entering one of the detector stacks. We use the *dE/dx* versus residual energy technique to determine the atomic number (*Z*), mass (*A*), and energy (*E*), of each cosmic ray. (**B**) Cross-plot of the sum of scaled energy losses of cosmic rays in detectors E1, E2, and E3 on the *y* axis versus the scaled energy loss in E4 on the *x* axis for a sample of particles stopping in E4, with both energies scaled by $(\sec\theta)^{-1/1.7}$, where θ is the angle of incidence through the instrument. Clear "bands" are seen for each element extending from calcium through nickel. Within some of the element bands, traces for individual isotopes of that element can be seen.

time except for intense solar-active periods, lasting for a few days each, when large fluxes of solar energetic particles exceeded the CRIS trigger rate capability. The instrument (Fig. 1A) uses a scintillating fiber hodoscope to determine particle trajectory and four stacks of silicon solid-state detectors to measure the energy loss (Δ*E*) and the total energy of cosmic-ray nuclei stopping in a detector stack. These measurements are used to identify particle charge, mass, and energy per nucleon (*5*). Data illustrating this method are shown in Fig. 1B, where we plot the energy loss (Δ*E*) versus the residual energy of nuclei stopping within a silicon detector. The elements are clearly separated into bands, and within an element band, subbands corresponding to the element's isotopes are evident.

Figure 2A is a mass histogram of the observed iron nuclei that entered the CRIS instrument through the scintillating optical fibers, penetrated the silicon detectors E1 through E3, and stopped in silicon detectors E4 through E8. These data were collected for 6142 days from 4 December 1997 to 27 September 2014. They have been selected for consistency among mass calculations using different detector combinations to reject nuclei that interacted within the instrument and other spurious events, as well as selections related to event quality (*14*).

Abundance of ^{60}Fe

Clear peaks are seen for masses from 54 to 58 amu (atomic mass units), with the exception of 57 amu, which is a shoulder on the 56 amu distribution. To the right of the 58 amu peak are 15 ^{60}Fe nuclei collected over this period, clearly separated from ^{58}Fe and located where ^{60}Fe should fall. These 15 events have a mean mass estimate of 60.04 amu and a standard deviation from the mean of 0.28 ± 0.05 amu, consistent with the 0.245 ± 0.001 amu measured for ^{56}Fe. The number of ^{56}Fe nuclei in this plot is 2.95×10^5, obtained from a Gaussian fit, and the total number of iron nuclei is 3.55×10^5. We have performed a number of tests to confirm that the 15 events are not a tail on the much more abundant ^{58}Fe distribution and have verified that in all respects tested, these events are not unusual (supplementary text and figs. S2 to S6). The strongest argument that they are ^{60}Fe

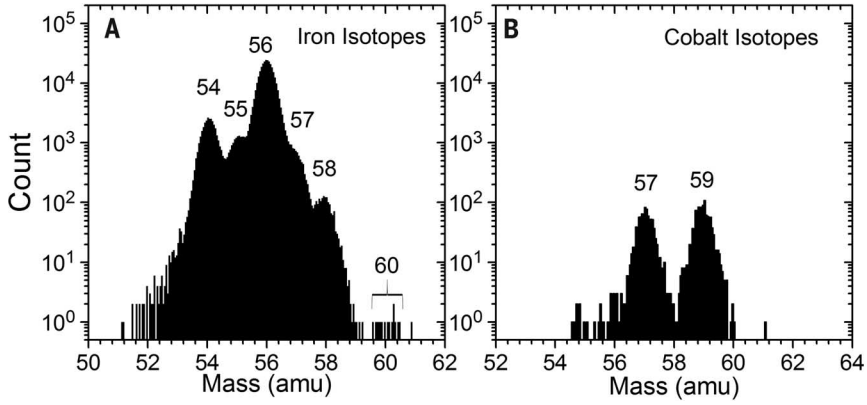

Fig. 2. Mass histograms of the observed iron and cobalt nuclei. (**A**) The mass histogram of iron nuclei detected during the first 17 years in orbit is plotted. Clear peaks are seen for masses 54, 55, 56, and 58 amu, with a shoulder at mass 57 amu. Centered at 60 amu are 15 events that we identify as the very rare radioactive ^{60}Fe nuclei. There are 2.95×10^5 events in the ^{56}Fe peak. From these data, we obtain an ^{60}Fe/^{56}Fe ratio of $(4.6 \pm 1.7) \times 10^{-5}$ near Earth and $(7.5 \pm 2.9) \times 10^{-5}$ at the acceleration source. (**B**) The mass histogram of cobalt isotopes from the same data set are plotted. Note that ^{59}Co in (B) has roughly the same number of events as are in the ^{58}Fe peak in (A). There is only a single event spaced two mass units to the right of ^{59}Co, whereas there are 15 events in the location of ^{60}Fe, which is two mass units from ^{58}Fe. This is a strong argument that most of the 15 nuclei identified as ^{60}Fe are really ^{60}Fe, and not a tail of the ^{58}Fe distribution.

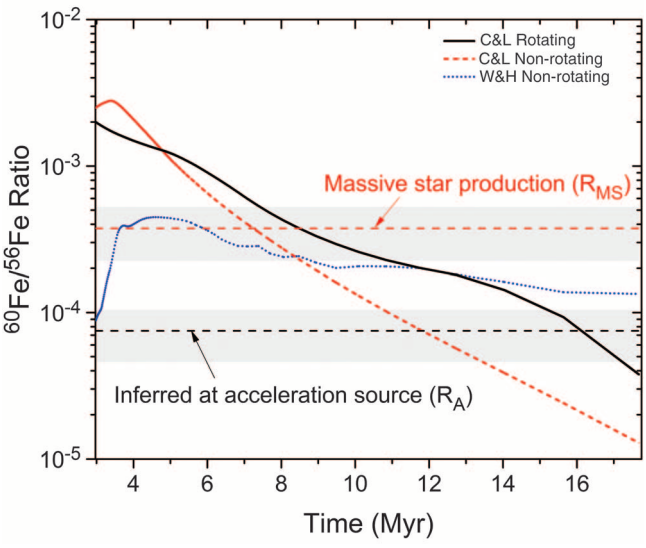

Fig. 3. Comparison of the $^{60}Fe/^{56}Fe$ ratio derived from measurements with models of supernova ejecta and stellar wind outflow in OB associations. Models of massive-star ejecta have been used to estimate the $^{60}Fe/^{56}Fe$ ratio evolution as a function of OB association age, including stellar lifetimes and radioactive decay of the ejected ^{60}Fe. The blue dotted curve shows the ratio for non-rotating stars using yields calculated by (*3*) (W&H); the red-dashed and black solid curves are for non-rotating and rotating stars, respectively, using yields calculated by (*4*) (C&L). The black dashed line is our estimated ratio (R_A) at the acceleration source derived from our measurements. Assuming that the composition at the acceleration source is 20% massive-star material and 80% normal interstellar medium material (supplementary materials), we obtain the massive-star production ratio (R_{MS}) (red dashed line). The shaded areas indicate uncertainties (not including the massive-star mix fraction uncertainty). We have compared the maximum predicted ratio (age ~3.4 My) with our measured ratio and estimate an upper limit to the time between nucleosynthesis and acceleration of several million years. Combining this with the previous measurement of ^{59}Ni (*2*), we conclude that the time between nucleosynthesis and acceleration is 10^5 years < T < several My.

nuclei and not spillover from ^{58}Fe is shown in Fig. 2B, which is a histogram of the neighboring cobalt (Z = 27) isotopes from the same data set. Note that ^{59}Co has roughly the same number of events as the ^{58}Fe peak. To the right of ^{59}Co, there is only a single event spaced by 2 amu. Similarly, we should expect only ~1 ^{58}Fe event to lie in the neighborhood of ^{60}Fe, but we see 15. It is also unlikely that these are spillover from ^{56}Fe since there is a clear separation between ^{58}Fe and the events that we identify as ^{60}Fe. Therefore, we conclude that at most, ~1 ± 1 of the 15 nuclei identified as ^{60}Fe could be spillover from lighter iron isotopes (supplementary text and fig. S1). Using the cosmic-ray propagation model described in (*15*), we have calculated the expected intensity ratio between secondary ^{60}Fe produced by fragmentation of heavier nuclei during interstellar transport and total Fe to be 2×10^{-6}, from which we conclude that only ~1 of the observed ^{60}Fe could be secondary. Thus, we have observed 13 ± 3.9 (statistical) ± 1 (systematic) = 13 ± 4.9 primary ^{60}Fe nuclei, giving measured ratios for $^{60}Fe/^{56}Fe$ and $^{60}Fe/Fe$ of $(4.4 \pm 1.7) \times 10^{-5}$ and $(3.7 \pm 1.4) \times 10^{-5}$, respectively.

These measured ratios need two small corrections. (i) Our data analysis eliminates particles that interact in the detector system. The cross-section for interaction of ^{60}Fe is slightly larger than that for ^{56}Fe, resulting in a correction factor of 1.009. (ii) Our analysis selects ^{60}Fe and ^{56}Fe with the same interval of depth of penetration in the detector. As a result, the energy interval for ^{60}Fe is smaller by a factor 0.960 than the interval for ^{56}Fe. Also, the ^{60}Fe energies per nucleon are slightly lower, although this has a very small effect because the Fe spectrum is quite flat at these energies (*15*). The resulting energy-interval correction is a factor of 1.042. Taken together, these require that the ratios be multiplied by a factor 1.051 (supplementary text). Thus, the corrected ratios near Earth are $^{60}Fe/^{56}Fe = (4.6 \pm 1.7) \times 10^{-5}$ and $^{60}Fe/Fe = (3.9 \pm 1.4) \times 10^{-5}$.

Using a leaky-box model, which accounts for radioactive decay of ^{60}Fe, nuclear interactions as the cosmic rays travel through space, and leakage out of the galaxy, these observations imply $^{60}Fe/^{56}Fe$ and $^{60}Fe/Fe$ ratios at the cosmic-ray acceleration source of $(7.5 \pm 2.9) \times 10^{-5}$ and $(6.2 \pm 2.4) \times 10^{-5}$, respectively (supplementary text).

Evidence of recent nucleosynthesis

Massive stars that undergo core-collapse exist primarily in localized groups called OB associations. The stars within these associations (or major subassociations) typically form at about the same time (within ~ 1 My), and associations have lifetimes of ~30 to 40 My (*16*). By that time, the stars with sufficient mass (>~10 $M_\odot$) have undergone core collapse. As the massive stars expel mass through high-velocity winds and supernova ejecta, superbubbles populated with the stellar wind material and ejecta are formed around the association (*16*). Calculations by Woosley and Heger (W&H) (*3*) and by Chieffi and Limongi (C&L) (*4*) estimate the production of ^{60}Fe and ^{56}Fe (outflow from stellar winds and supernova ejecta) from stars with initial masses from 12 to 120 $M_\odot$. Nearly all ^{60}Fe is in the supernova ejecta, not in the wind material. We have combined these results for a range of stellar masses with the lifetimes of the progenitor stars to determine the expected $^{60}Fe/^{56}Fe$ ratio in an OB association as a function of time. In Fig. 3, we plot the cumulative $^{60}Fe/^{56}Fe$ ratio of material injected into a superbubble as a function of time since the formation of the association at T = 0. We then derived the time that must have elapsed for this ratio to decrease to the value inferred from our cosmic-ray measurements due to the decay of the ^{60}Fe. Several different methods in which we compare our measured ratio with the modeling results lead us to conclude that an upper limit on the time between nucleosynthesis and acceleration is a few million years (supplementary text).

In previous work, on the basis of ACE-CRIS measurements of GCR ^{59}Ni and ^{59}Co, it was concluded that there is at least a 10^5-year delay between nucleosynthesis and cosmic-ray acceleration (*2*). Putting that lower limit together with this ^{60}Fe observation, we obtain a mean time (T) between nucleosynthesis and acceleration of 10^5 years < T < several My. This is quite consistent with what is expected in an OB association since a typical time between supernovae is ~1 My (*16*). In addition, the time delay between nucleosynthesis and acceleration indicates that the nuclei synthesized in a supernova are not accelerated by that supernova, but require at least one more nearby supernova to accelerate the material, on a time scale sufficiently short so that a substantial fraction of the ^{60}Fe has not decayed. The natural place for two or more nearby supernovae to occur within a few million years of each other is in OB associations. Thus, our observation of ^{60}Fe lends support to the emerging model of cosmic-ray origin in OB associations (*16*, *17*).

Using the mean lifetime of ^{60}Fe, we can also estimate the distance to the associations contributing ^{60}Fe GCRs at Earth. Assuming a diffusive propagation model, cosmic rays originate within a volume with radius $L = (D\gamma\tau)^{1/2}$ surrounding the solar system, where γ is the Lorentz factor and τ is the effective cosmic-ray lifetime. Assuming a diffusion coefficient of $D = 3.5 \times 10^{28}$ cm^2/s (*18*), and using γ and τ calculated for ^{56}Fe and ^{60}Fe (supplementary materials), we find that L_{56} = 790 pc and L_{60} = 620 pc. Because the volume scales as the cube of these diffusion lengths, the volume contributing to ^{60}Fe is only about half of that contributing to ^{56}Fe. There are >20 OB associations or major association subgroups that have been identified within 620 pc of the Sun, including the very large and nearby (<150 pc) Sco-Cen association subgroups—Upper Scorpius (with 83 OB stars), Upper Centaurus Lupus (with 134 OB stars), and Lower Centaurus Crux (with 97 OB stars) (*19*)—and the Orion OB1 association, modeled by (*20*) (with ~70 OB stars). These are very likely major contributors to the ^{60}Fe we have detected, owing to their size and proximity.

We can draw the model-independent conclusion that the detection of the radioactive supernova product ^{60}Fe surviving in cosmic rays implies

that the time required for acceleration and transport to Earth does not greatly exceed the ^{60}Fe half-life of 2.62 My. Our distance from the source of this nuclide cannot greatly exceed the distance that cosmic rays can diffuse over this time scale, which is ≲1 kpc.

Note added in proof: Additional detections of ^{60}Fe in deep-sea crusts in all major oceans of the world have recently been reported (*21*), strengthening the conclusions reached in (*9*). Also, additional detections of ^{60}Fe in lunar samples (*22*) strengthen the conclusion reached in (*12*, *13*).

REFERENCES AND NOTES

1. G. Rugel *et al.*, *Phys. Rev. Lett.* **103**, 072502 (2009).
2. M. E. Wiedenbeck *et al.*, *Astrophys. J.* **523**, L61–L64 (1999).
3. S. E. Woosley, A. Heger, *Phys. Rep.* **442**, 269–283 (2007).
4. A. Chieffi, M. Limongi, *Astrophys. J.* **764**, 21 (2013).
5. E. C. Stone *et al.*, *Space Sci. Rev.* **86**, 285–356 (1998).
6. W. Wang *et al.*, *Astron. Astrophys.* **469**, 1005–1012 (2007).
7. W. R. Binns, *Science* **334**, 1071–1072 (2011).
8. K. Knie *et al.*, *Phys. Rev. Lett.* **83**, 18–21 (1999).
9. K. Knie *et al.*, *Phys. Rev. Lett.* **93**, 171103 (2004).
10. C. Fitoussi *et al.*, *Phys. Rev. Lett.* **101**, 121101 (2008).
11. B. J. Fry, B. D. Fields, J. R. Ellis, *Astrophys. J.* **800**, 71 (2015).
12. L. Fimiani *et al.*, *43rd Lunar and Planetary Science Conference*, 1279 (2012).
13. L. Fimiani *et al.*, *45th Lunar and Planetary Science Conference*, 1778 (2014).
14. Materials and methods are available as supplementary materials on *Science* Online.
15. K. A. Lave *et al.*, *Astrophys. J.* **770**, 117 (2013).
16. J. C. Higdon, R. E. Lingenfelter, *Astrophys. J.* **590**, 822–832 (2003).
17. J. C. Higdon, R. E. Lingenfelter, *Astrophys. J.* **628**, 738–749 (2005).
18. N. E. Yanasak *et al.*, *Astrophys. J.* **563**, 768–792 (2001).
19. P. T. de Zeeuw, R. Hoogerwerf, J. H. J. de Bruijne, A. G. A. Brown, A. Blaauw, *Astron. J.* **117**, 354–399 (1999).
20. R. Voss, R. Diehl, J. S. Vink, D. H. Hartmann, *Astron. Astrophys.* **520**, A51 (2010).
21. A. Wallner *et al.*, *Nature* **532**, 69–72 (2016).
22. L. Fimiani *et al.*, *Phys. Rev. Lett.* **116**, 151104 (2016).

ACKNOWLEDGMENTS

This work was supported by NASA grants NNX08AI11G and NNX13AH66G for work performed at the California Institute of Technology, the Jet Propulsion Laboratory, and Washington University in St. Louis. Work done at Goddard Space Flight Center was funded by NASA through the ACE Project. We thank S. Woosley and J. Brown at the University of California Santa Cruz for providing modeling calculation data and for discussions about uncertainties in their calculations. We thank A. Chieffi at the Institute for Space Astrophysics and Planetology, Rome, Italy, for discussions on the uncertainties in the C&L calculations. Accelerator testing of the CRIS detectors was made possible by N. Anantaraman, R. Ronningen, and the staff at the National Superconducting Cyclotron Laboratory at Michigan State University, while H. Specht, D. Schardt, and the staff of the GSI heavy-ion accelerator in Darmstadt, Germany made possible the heavy-ion calibrations of the completed CRIS instrument. The data used are archived at NASA's Space Physics Data Facility (http://spdf.gsfc.nasa.gov) as data set ac_h2_cris and can be retrieved from this site by direct download or through the SPDF's CDAWeb data service.

SUPPLEMENTARY MATERIALS

www.sciencemag.org/content/352/6286/677/suppl/DC1
Materials and Methods
Supplementary Text
Figs. S1 to S6
References (*23*–*33*)

3 November 2015; accepted 18 March 2016
Published online 21 April 2016
10.1126/science.aad6004

PROTEIN DESIGN

De novo design of protein homo-oligomers with modular hydrogen-bond network–mediated specificity

Scott E. Boyken,[1,2,3] Zibo Chen,[1,2,4] Benjamin Groves,[5] Robert A. Langan,[1,2] Gustav Oberdorfer,[1,2,6] Alex Ford,[1,2] Jason M. Gilmore,[1,2] Chunfu Xu,[1,2] Frank DiMaio,[1,2] Jose Henrique Pereira,[7,8] Banumathi Sankaran,[9] Georg Seelig,[5,10] Peter H. Zwart,[9,11] David Baker[1,2,3]*

In nature, structural specificity in DNA and proteins is encoded differently: In DNA, specificity arises from modular hydrogen bonds in the core of the double helix, whereas in proteins, specificity arises largely from buried hydrophobic packing complemented by irregular peripheral polar interactions. Here, we describe a general approach for designing a wide range of protein homo-oligomers with specificity determined by modular arrays of central hydrogen-bond networks. We use the approach to design dimers, trimers, and tetramers consisting of two concentric rings of helices, including previously not seen triangular, square, and supercoiled topologies. X-ray crystallography confirms that the structures overall, and the hydrogen-bond networks in particular, are nearly identical to the design models, and the networks confer interaction specificity in vivo. The ability to design extensive hydrogen-bond networks with atomic accuracy enables the programming of protein interaction specificity for a broad range of synthetic biology applications; more generally, our results demonstrate that, even with the tremendous diversity observed in nature, there are fundamentally new modes of interaction to be discovered in proteins.

Hydrogen bonds play key roles in the structure, function, and interaction specificity of biomolecules. There are two main challenges facing de novo design of hydrogen-bonding interactions: First, the partially covalent nature of the hydrogen bond restricts polar hydrogen-containing donors and electronegative acceptors to narrow ranges of orientation and distance, and second, nearly all polar atoms must participate in hydrogen bonds—either with other macromolecular polar atoms, or with solvent—if not, there is a considerable energetic penalty associated with stripping away water upon folding or binding (*1*). The DNA double helix elegantly resolves both challenges; paired bases come together such that all buried polar atoms make hydrogen bonds that are self-contained between the two bases and have near-ideal geometry. In proteins, meeting these challenges is more complicated because backbone geometry is highly variable, and pairs of polar amino acids cannot generally interact as to fully satisfy their mutual hydrogen-bonding capabilities; hence, side-chain hydrogen bonding usually involves networks of multiple amino acids with variable geometry and composition, and there are generally very different networks at different sites within a single protein or interface preorganizing polar residues for binding and catalysis (*2*–*6*).

The modular and predictable nature of DNA interaction specificity is central to molecular biology manipulations and DNA nanotechnology (*7*, *8*), but without parallels in nature, it has not been evident how to achieve analogous programmable specificity with proteins. There are more polar amino acids than DNA bases, each of which can adopt numerous side-chain conformations in the context of different backbones, which allows for countless network possibilities. We hypothesized that by systematically searching through these network possibilities, it could be possible to design protein interfaces specified by regular arrays of DNA-like central hydrogen-bond networks with modular specificity analogous to Watson-Crick base pairing.

We began by developing a general computational method, HBNet, to rapidly enumerate all side-chain hydrogen-bond networks possible in an input backbone structure (Fig. 1A). Traditional protein design algorithms are not well suited for this purpose; the total system energy is generally expressed as the sum of interactions between pairs of residues for computational

[1]Department of Biochemistry, University of Washington, Seattle, WA 98195, USA. [2]Institute for Protein Design, University of Washington, Seattle, WA 98195, USA. [3]Howard Hughes Medical Institute, University of Washington, Seattle, WA 98195, USA. [4]Graduate Program in Biological Physics, Structure, and Design, University of Washington, Seattle, WA 98195, USA. [5]Department of Electrical Engineering, University of Washington, Seattle, WA 98195, USA. [6]Department of Computer Science and Engineering, University of Washington, Seattle, WA 98195, USA. [7]Institute of Molecular Biosciences, University of Graz, Humboldtstrasse 50/3, 8010-Graz, Austria. [8]Joint BioEnergy Institute, Emeryville, CA 94608, USA. [9]Molecular Biophysics and Integrated Bioimaging, Lawrence Berkeley National Laboratory, Berkeley, CA 94720, USA. [10]Berkeley Center for Structural Biology, Molecular Biophysics and Integrated Bioimaging, Lawrence Berkeley Laboratory, 1 Cyclotron Road, Berkeley, CA 94720, USA. [11]Department of Computer Science and Engineering, University of Washington, Seattle, WA 98195, USA. [12]The Center for Advanced Mathematics for Energy Research Applications, Lawrence Berkeley National Laboratories, 1 Cyclotron Road, Berkeley, CA 94720, USA.
***Corresponding author. Email: dabaker@u.washington.edu**

Science

Observation of the ^{60}Fe nucleosynthesis-clock isotope in galactic cosmic rays

W. R. Binns, M. H. Israel, E. R. Christian, A. C. Cummings, G. A. de Nolfo, K. A. Lave, R. A. Leske, R. A. Mewaldt, E. C. Stone, T. T. von Rosenvinge and M. E. Wiedenbeck

Science **352** (6286), 677-680.
DOI: 10.1126/science.aad6004originally published online April 21, 2016

Cosmic rays from a nearby supernova

Supernova explosions produce unstable isotopes, spreading them through space in the form of cosmic rays. Binns *et al.* used NASA's Advanced Composition Explorer spacecraft to search for previously undetected traces of ^{60}Fe in cosmic rays passing through the solar system. Seventeen years of observations detected just 15 ^{60}Fe nuclei—a small but statistically significant number. Because ^{60}Fe is radioactive, with a half-life of 2.6 million years, these nuclei must have formed relatively recently in a nearby supernova. The most likely candidates are massive stars in the Scorpius-Centaurus association.

Science, this issue p. 677

Science (print ISSN 0036-8075; online ISSN 1095-9203) is published by the American Association for the Advancement of Science, 1200 New York Avenue NW, Washington, DC 20005.